Brown Adipose Tissue: Multimodality Evaluation by PET, MRI, Infrared Thermography, and Whole-Body Calorimetry (TACTICAL-II)

Lijuan Sun [iD] [1]*, *Sanjay Verma* [iD] [2]*, *Navin Michael[3], Siew Pang Chan[4,5,6], Jianhua Yan[7],*
Suresh Anand Sadananthan[3], Stefan G. Camps[1], Hui Jen Goh[1], Priya Govindharajulu[1], John Totman[8],
David Townsend[8], Julian Pak-Nam Goh[9], Lei Sun[10], Bernhard Otto Boehm[11,12,13,14], Su Chi Lim[15], Siew Kwan Sze[16],
Christiani Jeyakumar Henry[1,17], Houchun Harry Hu[18], S. Sendhil Velan [iD] [2,3,19,20],
and Melvin Khee-Shing Leow[1,10,12,13]

Objective: This study aimed to compare the associations of positron emission tomography (PET), magnetic resonance (MR), and infrared thermography (IRT) imaging modalities with energy expenditure (EE) after brown adipose tissue (BAT) activation using capsinoid ingestion and cold exposure.

Methods: Twenty participants underwent PET-MR, IRT imaging, and whole-body calorimetry after capsinoid ingestion and cold exposure. Standardized uptake values (SUV) and the fat fraction (FF) of the supraclavicular brown adipose tissue regions were estimated. The anterior supraclavicular temperature (Tscv) from IRT at baseline and postintervention was measured. Two-hour post–capsinoid ingestion EE and post–cold exposure EE served as a reference to correlate fluorodeoxyglucose uptake, FF, and Tscv for BAT assessment. IRT images were geometrically transformed to overlay on PET-MR for visualization of the hottest regions.

Results: The supraclavicular hot spot identified on IRT closely corresponded to the area of maximal fluorodeoxyglucose uptake on PET images. Controlling for body weight, post–cold exposure Tscv was a significant variable associated with EE ($P = 0.025$). The SUV was significantly inversely correlated with FF ($P = 0.012$) and significantly correlated with peak of Tscv during cold exposure in BAT-positive participants ($P = 0.022$).

Conclusions: Tscv correlated positively with EE and was also significantly correlated with SUV after cold exposure. Both IRT and MR FF are promising methods to study BAT activity noninvasively.

[1] Clinical Nutrition Research Centre, Singapore Institute for Clinical Sciences, Agency for Science, Technology, and Research, National University Health System, Singapore. Correspondence: Melvin Khee-Shing Leow (melvin_leow@sics.a-star.edu.sg) [2] Laboratory of Molecular Imaging, Singapore Bioimaging Consortium, Agency for Science, Technology, and Research, Singapore [3] Singapore Institute of Clinical Sciences, Agency for Science, Technology, and Research, Singapore [4] Department of Medicine, Yong Loo Lin School of Medicine, National University of Singapore, Singapore [5] Cardiovascular Research Institute, National University Heart Centre, Singapore [6] College of Science, Health, and Engineering, La Trobe University, Melbourne, Australia [7] Molecular Imaging Precision Medicine Collaborative Innovation Center, Shanxi Medical University, Taiyuan, China [8] Clinical Imaging Research Centre, Agency for Science, Technology, and Research, National University of Singapore, Singapore [9] Department of Diagnostic Radiology, Tan Tock Seng Hospital, Singapore [10] Cardiovascular and Metabolic Disorders Program, Duke-National University of Singapore Medical School, Singapore [11] Genome Institute of Singapore, Agency for Science, Technology, and Research, Singapore [12] Lee Kong Chian School of Medicine, Nanyang Technological University, Singapore [13] Department of Endocrinology, Tan Tock Seng Hospital, Singapore [14] Imperial College London, London, UK [15] Department of Medicine, Khoo Teck Puat Hospital, Singapore [16] School of Biological Sciences, Nanyang Technological University, Singapore [17] Department of Biochemistry, Yong Loo Lin School of Medicine, National University of Singapore, Singapore [18] Department of Radiology, Nationwide Children's Hospital, Columbus, Ohio, USA [19] Department of Physiology, National University of Singapore, Singapore [20] Department of Medicine, National University of Singapore, Singapore.

Introduction

The prevalence of cardiovascular disease, hypertension, dyslipidemia, and type 2 diabetes is higher in individuals with obesity compared with lean individuals. With more than 650 million adults with obesity worldwide, more needs to be done to curb this pandemic. An emerging strategy capitalizes on brown adipose tissue (BAT) after the rediscovery of functional BAT in human adults (1-3). Activated BAT dissipates heat energy via nonshivering thermogenesis and contributes to energy expenditure (EE). Because BAT depots are sited fairly deep within the body, noninvasive imaging has been the preferred method of detection. Fluorine-18 fluorodeoxyglucose (^{18}F-FDG) positron emission tomography (PET) imaging has most commonly been used in combination with computed tomography (CT) to study and detect the metabolic activity of BAT (1). Because of concerns over radiation exposure, longitudinal PET-CT scanning for BAT studies in healthy individuals and children is not feasible. Other imaging methods, notably the magnetic resonance imaging (MRI) Dixon technique and infrared thermography (IRT), have been developed to facilitate noninvasive measurements of BAT without ionizing radiation (4,5). In adult humans, the dominant area of BAT is in the supraclavicular region (6,7). Activated BAT raises the anterior supraclavicular temperature (Tscv), which is detectable by IRT. Tscv, measured by IRT, is correlated to maximal glucose uptake on PET-CT images (8). MRI can measure fat fraction (FF - defined as the proportion of the acquired signal derived from fat protons) and T_2^*, which differ between BAT and WAT because of the former's high intracellular and extracellular water content and because of differences in vasculature and mitochondria (9-13).

Cold exposure is by far the most potent stimulus for BAT, and EE is increased after BAT activation (14). Capsinoids are capsaicin analogs found in nonpungent types of chili peppers (15). Dietary supplementation with capsinoids also leads to an increase in EE in adult humans via BAT activation (16,17). In our previous report, we found that EE was significantly increased after cold exposure and capsinoid ingestion in BAT-positive participants assessed through ^{18}F-FDG PET (18). The specific aim of this study was to evaluate BAT via a trimodality imaging approach, namely PET, magnetic resonance (MR), and IRT, coupled with EE via whole-body calorimetry (WBC) after BAT activation using capsinoid ingestion and cold stimuli. An important objective was to evaluate whether MR and/or IRT can serve as effective nonionizing alternatives to PET.

Methods

Participants

This prospective study, conducted from August 2016 to March 2017, involved healthy participants without type 2 diabetes mellitus and cardiovascular diseases. Current smokers and persons with special diets or on medications known to alter BAT metabolism were excluded. Participants had to be clinically and biochemically euthyroid, as confirmed by serum thyrotropin and free thyroxine concentrations within the normal ranges. The study was done in a tropical country with an equatorial climate characterized by relatively stable outdoor ambient temperatures and with a relatively stable day length across the entire year and was conducted according to the ethical guidelines of the Declaration of Helsinki. The Domain-Specific Review Board of National Healthcare Group, Singapore, approved all procedures, and the study was registered on ClinicalTrials.gov (TACTICAL-II,

identifier NCT02964442). Written informed consent was obtained from all participants before participation.

Study design

The participants attended two separate visits for PET-MR and two separate visits for WBC/IRT to assess the effects of capsinoid ingestion and cold exposure. Visits were separated by a minimum washout period of 48 hours to minimize carry-over effects. Capsinoid capsules (12 mg; eight gel capsules) were provided by Ajinomoto Co., Inc. (Tokyo, Japan). The composition details were described previously (19). Cold stimulation was achieved using a cooling vest with a fixed temperature of 14.5°C (Polar Products, Stow, Ohio). The participants were asked to refrain from caffeine and alcohol intake and any vigorous physical activity a day before the study. The study protocol and flowchart were described previously (18).

Screening measurements

Standing height (in meters) was measured with a stadiometer, and body weight (in kilograms) was measured with a bioelectrical impedance analysis device (Tanita BC-418; Tanita Corp., Tokyo, Japan), which also includes a digital weighing scale. Body fat, fat mass, and fat-free mass were measured by dual-energy x-ray absorptiometry (QDR 4500A; Hologic, Inc., Waltham, Massachusetts).

Blood analysis

Screening blood samples were sent for renal, liver and thyroid function tests. High-density lipoprotein (HDL), triglycerides (TG), fasting glucose, and fasting insulin were measured using the Cobas e311 analyzer (Roche Diagnostics, Basel, Switzerland). Serum nonesterified fatty acids (NEFA) were measured by using a commercially available enzymatic colorimetric assay (Wako Chemicals, Osaka, Japan). Homeostatic model assessment of insulin resistance (HOMA-IR) was measured from fasting insulin and fasting glucose as (fasting insulin [microunits per milliliter] × fasting glucose [millimoles per liter])/22.5.

EE and IRT

Participants, wearing light cotton singlets and Bermuda shorts only, were seated in an upright posture on a chair with their head positioned neutrally and their arms adducted. A thermal-imaging camera (FLIR T440; FLIR Systems, Wilsonville, Oregon) was mounted on a tripod, placed in front of the participant, and positioned at neck height, 1 m from the participant's face. After a 10-minute acclimatization period and a 45-minute measurement of the baseline resting metabolic rate, baseline thermal images were recorded. After the baseline measurement, participants were asked to ingest the capsinoid capsules during the first WBC/IRT visit, or to wear the cooling vest during the second WBC/IRT visit, inside the WBC room for a 2-hour measurement. The cooling vest was wrapped around the torso, leaving the anterior supraclavicular region exposed. All IRT video recordings were acquired over a standardized recording period of 1 second (30 frames per second), whereby anterolateral views of the anterior supraclavicular region were captured bilaterally. The thermal images were recorded every 15 minutes for 2 hours. The participants were requested to remain as still as possible with their shoulders apposed squarely against the back of the chair to minimize movement within the image frames during thermal video recordings. Thermal imaging was performed in

the same room as the WBC EE measurements at a constant ambient temperature of 24ºC. Resting metabolic rate and change in EE during the 2-hour intervention were calculated based on methodology established in a previous study (20).

PET-MR

After fasting for 10 to 12 hours, the participants arrived at the Clinical Imaging Research Centre. An indwelling cannula was inserted into a forearm vein by a registered nurse after a 10-minute rest, and fasting blood glucose was measured. During the first visit, participants were asked to ingest capsinoids 30 minutes before the scan. During the second visit, participants were asked to wear the cold vest after arrival. Because of the logistics of scanner availability, the duration of the prescan cooling was not fixed and ranged between 51 and 162 minutes. During both visits, participants were given an intravenous injection of ^{18}F-FDG (3 mCi) 20 minutes before the start of the scans. The scans were performed on a hybrid 3-T PET-MR system (Biograph mMR; Siemens Healthineers, Erlangen, Germany) for 80 minutes. Three-dimensional (3D) T2-weighted anatomical images were acquired using the following: repetition time (TR) = 1,300 milliseconds; echo time (TE) = 120 milliseconds; field of view = 384 mm × 384 mm; and matrix size = 192 × 192. A 3D multipoint (10 echoes) Dixon sequence was used for the water-fat imaging at the start and end of the scan with the following parameters: TR = 15 milliseconds; 10 echo times = 1.23, 2.46, 3.69, 4.92, 6.15, 7.38, 8.61, 9.84, 11.07, and 12.30 milliseconds; flip angle = 4°; field of view = 384 mm × 384 mm; matrix size = 192 × 192; bipolar readout mode and 112 sections with 2-mm thickness. Total acquisition time for the multipoint Dixon sequence was approximately 4.49 minutes. All imaging sequences had anatomical coverage of the neck, supraclavicular region, and the apexes of the lung.

Analysis of IRT

Recorded as a radiometric infrared video using the FLIR ResearchIR software version 3.3 (FLIR Systems, Wilsonville, Oregon), the thermal data were analyzed with a modified seeded region growing technique using a semiautomated algorithm to detect the hot regions overlaying the supraclavicular brown adipose tissue (sBAT). At the start of the algorithm, a bounding box encompassing likely sBAT depots was manually drawn on the first frame of the infrared video, from which the pixel of the maximum temperature value was automatically selected as the "seed." The seed initialized the region of interest (ROI), which was iteratively grown by comparing all unallocated neighboring pixels to the region. A fixed threshold was optimized for all the participants to achieve reliable segmentation. With the same algorithm, all frames in a single infrared video were calibrated by detecting and using circular aluminum foil disks that were placed on the subject's skin (diameter of 5 mm; four on the upper thorax demarcated by 5 × 5 cm²). The temperature of the skin overlying the sternum, a region devoid of BAT, served as a good reference. The median frame out of the 1-second (30 frames) video was subsequently used to represent the particular time point at which the video was taken and the ROI calculated. The ROI of the hot region, as delineated by this algorithm, served to identify potential sBAT depots.

Analysis of PET-MR

The multi-echo complex data were fitted using Levenberg-Marquardt nonlinear fitting and using the seven-peak fat model with the following equations:

$$\left|S_n\right| = \left|\left(M_w + c_n M_f\right) \cdot e^{-R_{2eff}^* TE_n}\right| ; and$$

$$\left|S_n\right| = \left|\left(M_w \cdot e^{-R_{2w}^* TE_n} + c_n M_f \cdot e^{-R_{2f}^* TE_n}\right)\right|.$$

R_{2w}^* and R_{2f}^* are the R_2^* of water and fat independently, and R_{2eff}^* is the effective R_2^* of both water and fat; c_n is the complex coefficient, defined as $c_n = \sum_1^7 w_i e^{j(2\pi\Delta f_i TE_n)}$, for a seven-peak fat model; and w_i and f_i are the weighting factor and the resonance frequency offset of the fat peak, respectively (21). The initial guesses for the water and fat signal fraction were obtained based on the Dixon composition of the first two echoes. A multi-step adaptive nonlinear fitting approach was used to update the water and fat signal fraction and R_2^* values (22). Pixelwise quantification of FF was performed from fat and water maps. The standardized uptake value (SUV) was calculated as previously described (23).

An affine-based registration method was used to register MR and PET images (24). The initial mask was generated by the rolling ball background subtraction algorithm followed by the percentile-based automatic thresholding method. Erosion and dilation were performed to remove the extra unwanted regions and to fill the holes inside the initial mask (25). The final mask was applied to exclude the unwanted region and background from MR and PET images. sBAT depots were manually segmented based on anatomical information in multiple section images of registered MR and PET images using ITK-SNAP (version 3.6.0) and under close guidance of an experienced radiologist (26). A lower threshold of 40% of FF values was used to exclude the muscle and bone marrow (27).

Integration of PET, MR, and IRT

A 3D-volume rendering of MR and PET images was performed using α blending (28). A one-dimensional transfer function was defined using the α (luminance) of each voxel of the volume, with an optimal global offset for better visualization. The optimal two-dimensional (2D) projection was obtained in coronal orientation by navigating through MR and PET volumes. The IRT map was selected based on the maximum mean temperature in the sBAT region. The IRT map was wrapped on to the 2D overlaid image of PET-MR. Control-point pairs were identified manually based on the anatomical location of sBAT, left and right superolateral apexes, acromioclavicular apexes, and sternal apex using the *cpselect* function of MATLAB 2016b (MathWorks, Natick, Massachusetts) from IRT, MR, and PET and their edge images. The *Fitgeotrans* function was used to wrap the IRT and PET-MR maps using the *affine* transformation model. Finally, the wrapped IRT map was overlaid on the PET-MR data to visualize the overlap of the hottest sBAT region and maximal glucose uptake.

Data analysis

The association among the relevant variables was examined using the Pearson correlation. We performed a confirmatory analysis using a generalized structural equation model (29), while taking the different visits and sequence of measurements into account. The analysis was adjusted with the duration of cold exposure and demographics (sex, age, body weight, and percentage of body fat). The FF was measured at the start and end of the scan (80 minutes), whereas the SUV was integrated over the 80-minute scan on the same visit. The IRT Tscv was measured at baseline, peak, and 120 minutes on a separate visit. We used the linear mixed-effects model to evaluate the main effects of the treatment type (capsinoids vs. cold exposure) and to evaluate the BAT status of participants (BAT-positive vs. BAT-negative) as well as their interactions, while controlling for baseline measurements. Data are

TABLE 1 Participant characteristics[a]

	All participants	Male participants	Female participants	P value[b]
n	20	8	12	…
Age, y	25.9 ± 4.1	25.8 ± 4.1	25.9 ± 4.3	NS
Height, cm	168.5 ± 8.9	175.0 ± 5.4	164.2 ± 8.2	0.004
Weight, kg	62.5 ± 12.6	70.5 ± 12.7	57.1 ± 9.8	0.015
BMI[c]	21.7 ± 2.5	22.9 ± 3.0	20.9 ± 1.8	NS
Body fat, %	29.2 ± 8.0	23.4 ± 6.6	33.2 ± 6.3	0.004
Fat mass, kg	18.4 ± 7.5	17.1 ± 7.6	19.3 ± 7.6	NS
Fat-free mass, kg	43.6 ± 9.5	53.0 ± 6.9	37.4 ± 4.3	<0.001
RMR, kcal/d[d]	1,533 ± 271.0	1,752.5 ± 245.5	1,386.7 ± 173.6	0.001

[a]Values are mean ± SEM.
[b]P values represent Student t test between male and female participants.
[c]BMI calculated as body weight (in kilograms) divided by height (in meters squared).
[d]Values represent average RMR from two whole-body calorimeter study visits.
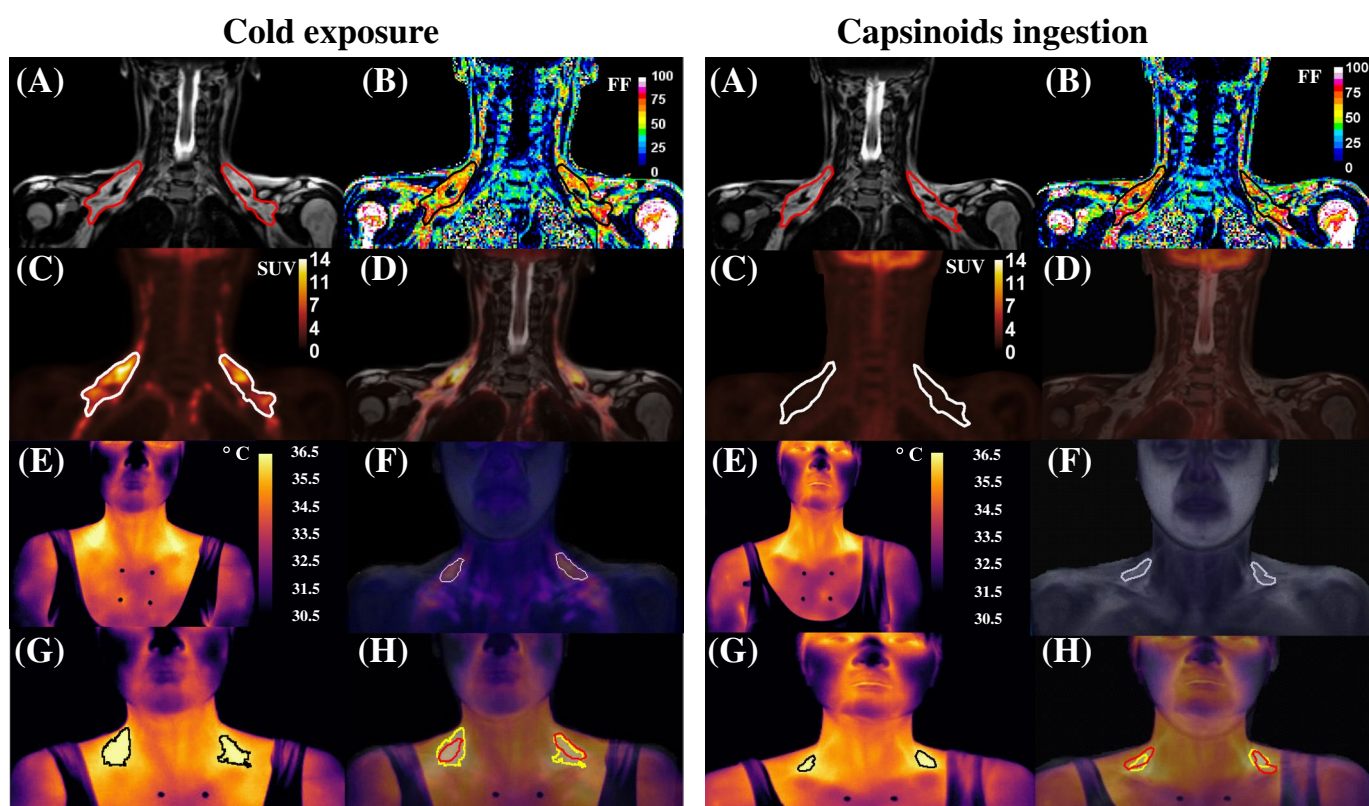NS, not significant; RMR, resting metabolic rate.

Cold exposure

Capsinoids ingestion

Figure 1 Representative images of a brown adipose tissue (BAT)–positive participant after cold exposure and capsinoid ingestion. (**A,B,C**) T2-weighted anatomical image showing the supraclavicular brown adipose tissue (sBAT), the fat fraction (FF) map in which sBAT is highlighted (color scale shows values of FF in percentages), and the fluorine-18 fluorodeoxyglucose (^{18}F-FDG) positron emission tomography (PET) map with a color scale showing standardized uptake values (SUV). (**D**) PET overlaid on the magnetic resonance (MR) image. (**E**) Infrared thermography (IRT) map with a color bar showing the temperature in degrees Celsius. (**F**) 2D projected PET image overlaid on the MR image, with the regions of interest (ROI) showing the maximum glucose uptake within sBAT. (**G**) Wrapped IRT image on the PET-MR image, with ROI showing the maximum temperature within sBAT. (**H**) Overlaid images of IRT and PET-MR highlighting the maximum glucose uptake (red) and hot (yellow) regions within sBAT.

presented as mean (SEM) unless otherwise stated. $P < 0.05$ was considered statistically significant. A statistical analysis was performed in Stata software MP version 14.0 (StataCorp LLC, College Station, Texas) for the confirmatory analysis, and another statistical analysis was performed in SPSS Statistics software version 23 (IBM Corp., Armonk, New York).

Results

Characteristics of participants

The data of 20 healthy participants (age: 25.9 [4.1] years; number of male participants: 8) were analyzed. Their BMI and body fat percentage were 21.7 (2.5) and 29.2% (8.0%), respectively (Table 1). There was a significant sex difference in body weight (male participants: 70.5 [12.7] kg vs. female participants: 57.1 [9.8] kg; $P=0.02$). The female participants were found to have a significantly higher body fat percentage than their male counterparts (33.2% [6.3%] vs. 23.4% [6.6%]; $P<0.004$). PET-MR data from two female participants were not included because of their motion during part of the MR scan, which led to inaccurate FF computations. Thus, the FF map was analyzed with only 18 participants. Other analyses that did not require the FF map were done on the full sample of 20 participants.

BAT imaging using PET, MR, and IRT, which show area overlaps

Representative images of PET, MR, and IRT from a participant after cold exposure and capsinoid ingestion are shown in Figure 1. The ROI around the sBAT was drawn on a coregistered T2-weighted anatomical image showing the FF and SUV maps (Figure 1A-1C). The PET images were overlaid on anatomical MR images (Figure 1D) to achieve better visualization and functional information. IRT images (Figure 1E) also showed higher temperatures after cold exposure compared with after capsinoid ingestion. The 2D projected PET image overlaid on the MR projected image is shown in Figure 1F, with the ROI showing maximum glucose uptake around sBAT. The uptake was higher after cold exposure compared with after capsinoid ingestion. The ROI was drawn to show the maximum temperature

within sBAT on the wrapped IRT image, as shown in Figure 1G. The overlaid image of IRT and PET-MR (Figure 1H) highlights the maximum glucose uptake and hottest regions within sBAT. A significant anatomical overlap of the hottest regions and maximal glucose update was observed.

BAT imaging assessments before and after capsinoids and cold

The BAT imaging parameters from the three modalities before and after the interventions for all the participants are shown in Table 2. We also evaluated these parameters after stratifying the participants into BAT-positive and BAT-negative groups based on the PET uptake, as defined previously (18). The mean cutoff SUV for dividing participants into BAT-positive and BAT-negative groups was 2.0. In BAT-positive, but not in BAT-negative, participants, the SUV after cold exposure was significantly higher versus after capsinoid ingestion. There was significant interaction between treatment and participant status ($P=0.022$). The rest of the variables (FF, Tscv, and EE) had no significant interaction between treatment and participant status. The respective main effects of treatment and of participant status are reported in Table 3.

BAT imaging assessments and EE

The confirmatory analyses were adjusted for body weight only because it was significantly associated with EE at 2 hours. After cold exposure, Tscv at 2 hours was found to have a positive and significant ($P=0.025$) correlation with EE at 2 hours, with adjustment for body weight and duration of cold exposure. Other things being equal, a 1°C increase in Tscv reflected an increase in EE by almost 206 kcal/d (Table 4). However, after capsinoid ingestion, Tscv did not show any significant correlation with EE at 2 hours, with adjustment for body weight (Table 4). The SUV and FF did not show any significant association with EE after both capsinoid ingestion and cold exposure.

Effects of cold duration on SUV and FF

The SUV after cold stimulation was not found to be associated with the duration of cold exposure (Figure 2A), whereas the FF was found to be negatively associated, as shown in Figure 2B. A significant negative correlation was found between SUV and the end-of-scan FF after we adjusted for body weight and duration of cold exposure (Figure 2C).

Relationship between PET SUV and maximum IRT Tscv after cold exposure

There was a statistically significant correlation between the PET SUV and the maximum Tscv ($r=0.651$; $P=0.022$). The correlation between PET the SUV against the Δ Tscv was just short of statistical significance (maximum Tscv− baseline Tscv) ($r=0.574$; $P=0.051$) (Figure 3).

Relationship between imaging parameters and blood lipids and HOMA-IR

Plasma NEFA was positively correlated with the SUV ($P=0.01$). Plasma HDL and NEFA were negatively correlated with FF, whereas TG and FF were positively correlated after cold exposure. HOMA-IR correlated positively with the FF of BAT (Table 5).

TABLE 2 Summary of outcomes of SUV, FF, IRT Tscv, IRT Tref, and EE after capsinoid ingestion and cold exposure in all participants[a]

	Capsinoid ingestion	Cold exposure
SUV	1.07 ± 0.05	1.51 ± 0.18[b]
FF (%)		
Start of scan	76.30 ± 1.36	74.59 ± 1.55
End of scan	74.63 ± 1.33	75.33 ± 1.54
IRT Tscv (°C)		
Baseline	35.28 ± 0.09	35.30 ± 0.10
120 minutes	35.23 ± 0.10	35.25 ± 0.14
IRT Tref (°C)		
Baseline	33.46 ± 0.20	33.56 ± 0.13
120 minutes	33.73 ± 0.18	32.18 ± 0.55[c]
EE (kcal/d)		
Baseline	1,529.85 ± 61.19	1,567.50 ± 70.74
120 minutes	1,648.55 ± 62.96[c]	1,775.10 ± 77.46[c]

[a]Values are mean±SEM; SUV and FF values calculated from 18 participants; IRT Tscv, IRT Tref, and EE values calculated from 20 participants.
[b]Different from capsinoid ingestion; tested using paired *t* test; $P<0.05$.
[c]Different from baseline within same treatment group; tested using paired *t* test; $P<0.05$.
[d]Tref, chest reference temperature; EE, energy expenditure; FF, fat fraction; IRT, infrared thermography; SUV, standardized uptake value; Tref, chest reference temperature; Tscv, anterior supraclavicular temperature.

TABLE 3 Summary of outcomes of SUV, FF, IRT Tscv, IRT Tref, and EE after capsinoid ingestion and cold exposure in BAT-positive and BAT-negative participants

	BAT-positive participants		BAT-negative participants		Treatment effects, P^d	Participant status effects, P^d	Treatment × participant status interactions, P^d
	Capsinoid ingestion	Cold exposure	Capsinoid ingestion	Cold exposure			
SUV	1.08 ± 0.06	1.78 ± 0.24[c]	1.07 ± 0.11	1.00 ± 0.11	0.053	0.082	0.022
FF (%)					0.524	0.735	0.163
Start of scan	77.22 ± 1.80	74.67 ± 2.06	74.47 ± 1.92	75.40 ± 2.00	…	…	…
End of scan	74.34 ± 1.83	74.85 ± 2.15	75.17 ± 1.81	76.23 ± 2.05	…	…	…
IRT Tscv (°C)					0.795	0.143	0.221
Baseline	35.33 ± 0.08	35.33 ± 0.06	35.19 ± 0.21	35.25 ± 0.23	…	…	…
120 minutes	35.31 ± 0.08	35.40 ± 0.13	35.10 ± 0.22	35.04 ± 0.27	…	…	…
IRT Tref (°C)							
Baseline	33.50 ± 0.28	33.50 ± 0.17	33.41 ± 0.30	33.64 ± 0.20	…	…	…
120 minutes	33.74 ± 0.26	32.08 ± 0.85	33.71 ± 0.23	32.33 ± 0.58	…	…	…
EE (kcal/d)					0.005	<0.001	0.146
Baseline	1,486.50 ± 95.64	1,573.75 ± 87.98	1,558.75 ± 81.91	1,558.13 ± 125.27	…	…	…
120 minutes	1,706.33 ± 80.22	1,840.58 ± 100.91	1,561.88 ± 99.71	1,676.88 ± 120.06	…	…	…

[a]SUV calculated from PET, integrated in 80 minutes, and coregistered with MR in region of interest supraclavicular area; FF from MR at start of scan was 20 minutes after capsinoid ingestion or 1 to 2 hours of cold exposure. End of scan calculated at end of 80 minutes; Tscv, Tref, and EE obtained at baseline and at end of study at 120 minutes in whole-body calorimetry/IRT sessions.
[b]Values are mean ± SEM; SUV and FF values calculated from 18 participants (11 BAT-positive participants and 7 BAT-negative participants); IRT Tscv, IRT Tref, and EE values calculated from 20 participants (12 BAT-positive participants and 8 BAT-negative participants).
[c]Different from capsinoid ingestion; tested using paired t test; $P < 0.05$.
[d]Treatment effects, participant status effects, and interactions between treatment and participant status were tested using linear mixed-effects model, controlling for baseline measurements.
BAT, brown adipose tissue; EE, energy expenditure; FF, fat fraction; IRT, infrared thermography; MR, magnetic resonance; PET, positron emission tomography; SUV, standardized uptake value; Tref, chest reference temperature; Tscv, anterior supraclavicular temperature.

TABLE 4 Regression results of EE with imaging parameters (SUV, FF, and IRT Tscv) after capsinoid ingestion and cold exposure

	Capsinoid ingestion			Cold exposure		
	Coefficient	95% CI	*P*	Coefficient	95% CI	*P*
SUV	218.5	−298.9 to 735.8	0.382	17.2	−165.5 to 199.9	0.843
Body weight (kg)	14.8	6.2 to 23.4	0.002	19.9	9.5 to 30.2	0.001
Constant	477.6	−89.6 to 1,044.7	0.093	482.7	−153.0 to 1,118.4	0.126
FF (%)	−1.94	−20.9 to 17.0	0.83	−1.87	−27.7 to 23.9	0.88
Body weight (kg)	16.7	8.9 to 24.6	<0.001	19.8	7.4 to 32.2	0.004
Constant	733.7	−676.1 to 2,143.5	0.29	660.2	−1,034.4 to 2,354.8	0.42
Tscv (°C)	156.3	−47.7 to 360.2	0.124	205.5	28.6 to 382.4	0.025
Body weight (kg)	18.1	11.1 to 25.1	<0.001	22.6	14.4 to 30.9	<0.001
Constant	−4,999.1	−12,331.1 to 2,332.9	0.11	−6,894.9	−13,311.4 to −478.5	0.037

SUV and FF values calculated from 18 participants. SUV, calculated from PET, was integrated in 80 minutes; FF, calculated from MR imaging, at end of the scan was integrated at 80 minutes; Tscv from IRT analysis was integrated in 120 minutes in supraclavicular region; and average EE was integrated in 120 minutes. Analysis adjusted with body weight (kilograms).
EE, energy expenditure; FF, fat fraction; IRT, infrared thermography; MR, magnetic resonance; PET, positron emission tomography; SUV, standardized uptake value; Tscv, anterior supraclavicular temperature.
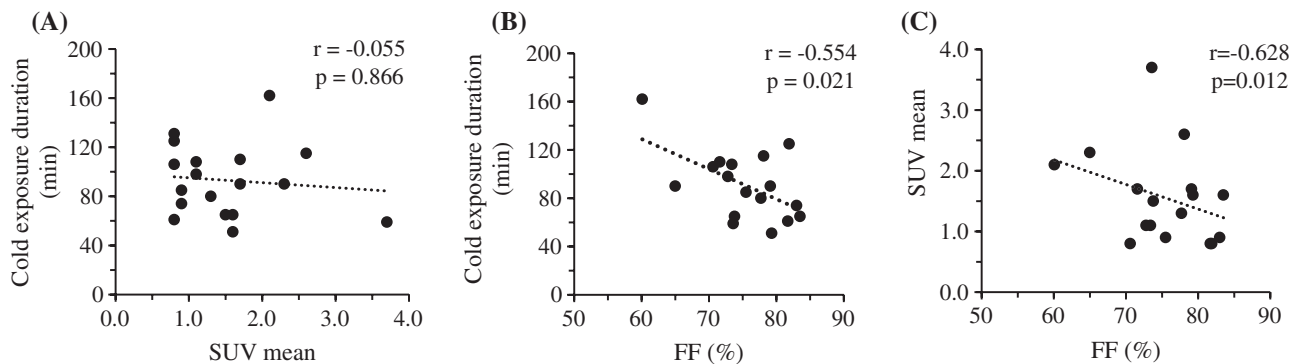

Figure 2 Correlation between (**A**) standardized uptake value (SUV) and (**B**) fat fraction (FF) with duration of cold exposure in 18 participants. (**C**) Correlation between SUV and FF after adjustment for cold exposure duration and body weight in 18 participants.
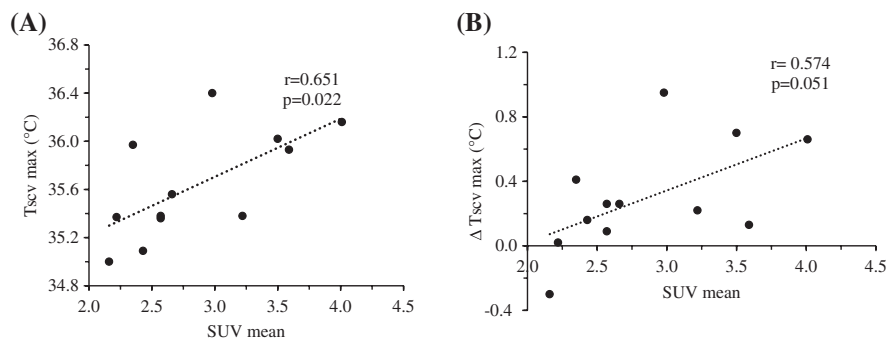

Figure 3 Correlations between the positron emission tomography (PET) mean standardized uptake value (SUV) and the (**A**) infrared thermography (IRT) maximum anterior supraclavicular temperature (Tscv max) and (**B**) Tscv max change from baseline (Δ Tscv max) in PET brown adipose tissue (BAT)–positive participants (*n* = 12).

TABLE 5 Summary of imaging parameters' relationship with blood metabolic markers after cold exposure

Blood parameter	SUV β	SUV P	FF (%) β	FF (%) P	Tscv (°C) β	Tscv (°C) P
HDL (mmol/L)	0.04	0.88	−0.52	0.02	0.19	0.41
TG (mmol/L)	−0.11	0.68	0.52	0.04	0.07	0.78
NEFA (mmol/L)	0.63	0.01	−0.58	0.01	0.21	0.41
HOMA-IR	−0.04	0.87	0.61	0.01	0.19	0.45

Correlations between imaging parameters and plasma concentration parameters at 120 minutes after cold exposure and HOMA-IR, calculated on the cold-exposure whole-body calorimetry/infrared thermography visit, with adjustment for sex.
FF, fat fraction; HDL, high-density lipoprotein; HOMA-IR, homeostatic model assessment of insulin resistance; NEFA, nonesterified fatty acid; SUV, standardized uptake value; TG, triglyceride; Tscv, anterior supraclavicular temperature.

Discussion

Adult humans have first been found to possess functional BAT dating back to more than 3 decades ago (30). During the era of the late 1970s and 1980s, functioning BAT was proven to exist in adult humans (31,32). Enigmatically, the erroneous view that BAT is absent in adults perpetuated over many years, nonetheless, until the more recent simultaneous rediscovery of the presence of functional depots of BAT in humans (1-3), leading to a revival of interest in BAT as a potential target for increasing EE to combat metabolic disease. PET has already been instrumental in the identification of BAT in humans (33) and is routinely used in functional characterization of BAT activity in rodents (34,35). PET relies on the uptake of the radio-labeled tracer 2-deoxy-2-^{18}F-FDG, an analog of glucose, which is taken up by metabolically active tissues. However, the exposure to ionizing radiation limits the wider applicability of PET for investigating BAT activity in the general population.

This study was the first to measure BAT activity in humans using three imaging modalities, namely PET, MR, and IRT, after sympathetic nervous system activation via capsinoid ingestion and cold exposure. Our key finding was that participants identified as BAT-positive and BAT-negative by PET differed distinctively in both their thermal responses as well as their elevation of EE after cold exposure. BAT-positive participants, but not BAT-negative participants, had elevated EE after both capsinoid ingestion and cold exposure. Although both groups experienced a significant drop in the reference temperature after cold exposure, a trend exists in which the BAT-positive participants were protected from a decline in Tscv. In the pooled participants, the Tscv after 2 hours of cold exposure also had significant correlation with EE, indicating that an increase in Tscv could provide a reliable estimate of EE increase after BAT activation. The SUV and high-resolution, MR-based FF imaging allowed supraclavicular and cervical BAT to be anatomically localized and visualized. IRT, being a surface imaging modality, offered limited insights into the localization and amount of BAT but was sensitive to functional BAT activity. The correlation between SUV and the maximum IRT Tscv is statistically significant, thereby supporting the use of IRT as an imaging modality for activated BAT.

In our experimental paradigm for cold exposure, participants wore the cooling vest before the PET-MR scan but not during the scan because the vest was not MRI compatible. Because the ^{18}F-FDG uptake after cold exposure was suggestive of increased BAT activity in the BAT-positive participants, we expected the FF to decline during the scan because of increased consumption of lipid substrates during BAT thermogenesis. To understand the lack of change in the FF between the start and end of the scan, we evaluated the association of the duration of cold exposure with the FF and SUV. We found that the FF, but not the SUV was inversely associated with the duration of cold exposure. These results suggest that cold may induce an initial spike in glucose uptake in BAT, but sustained cold exposure may increase reliance on fat as a substrate for thermogenesis. After controlling for the duration of cold exposure, the FF measured after cold exposure at the end of the scan at 80 minutes varied inversely with the SUV, consistent with previous studies (27,36,37), indicating that the FF is indeed related to functional BAT activity.

In addition to the role of dynamic changes in FF in evaluating BAT activity, the TG content of the supraclavicular depot has been found to be positively associated with insulin resistance and risk of diabetes (38). In concordance with this, we also found the FF after cold exposure to be positively associated with HOMA-IR and TG and negatively associated with HDL cholesterol. We also found a negative association with NEFA levels, which could be a reflection of increased usage of plasma NEFA for BAT thermogenesis. Recent studies have investigated T_2^* to evaluate differences between supraclavicular and gluteal adipose tissues and variable number of gradient echoes (13). In addition, the fat water spectral model, which includes susceptibility-induced frequency variation has been evaluated (12). In this study, we did not investigate the metabolic correlation with T_2^* values for BAT-positive and BAT-negative participants.

Capsinoid ingestion was linked to an increase in EE in BAT-positive participants, although the ^{18}F-FDG uptake after capsinoid ingestion was notably low in both groups. Importantly, we had earlier published data supporting a subthreshold increase in the SUV after capsinoid ingestion (18). Neither group experienced any significant changes in Tscv or FF after capsinoid ingestion. These results indicate a low sensitivity for these three imaging modalities to detect functional changes in sBAT after capsinoid ingestion. More studies are required to ascertain if the sBAT activity in capsinoid-induced elevation in EE is clinically significant.

Our study has a few limitations. The perceived fear of ionizing radiation associated with PET led to a small sample size, which limited the power to detect significant changes in the imaging parameters after different interventions. We also lacked a PET-MR scan at ambient temperature to compare the difference between ambient temperature and cold exposure. The logistics of scanner availability led to a variation in cold exposure duration between participants. This probably contributed to the lack of correlation between the FF and maximum Tscv, which can be further explored in future studies. We only used the front Tscv to correlate with the SUV and FF, but this approach may miss BAT localized over the left and right neck regions. A more sophisticated IRT (e.g., 3D and four-dimensional IRT with improved segmentation) might be required to assess changes in Tscv with finer details after BAT activation.

Our present study demonstrated the feasibility to detect BAT activation in both sexes by cold exposure and capsinoid ingestion using multiple imaging modalities: PET, MRI, and IRT. This sets the stage for future prospective BAT studies to elucidate sex differences. The anatomical information from MRI and functional information from IRT provide a

nonionizing alternative to PET-CT for BAT assessments. Radiometric sensors are now able to distinguish changes of 0.01ºC while the resolution of images is improving. Combined with an automated analysis, the variability of IRT between individuals should be further reduced. Given the low cost of IRT, the above improvements will be useful for establishing IRT as a valid method of measuring sBAT activity in the wider population. MRI also provides information beyond the anatomical localization of BAT. Although PET and IRT can only be used to assess the acute effect of thermogenic stimuli, the FF of the supraclavicular region can provide unique insight into longer-term metabolic health.

Conclusion

IRT is a valid imaging method for BAT, in preference over PET-CT. IRT has potential practical utility in terms of facilitating research in the evaluation of therapeutics (i.e., nutraceuticals and pharmaceuticals) in large clinical populations because it is of relatively low cost, is convenient, and is safe for serial applications. Successful establishment of IRT and MR FF as effective BAT imaging modalities will promote their use in the monitoring and follow-up of BAT-based interventions among patients and healthy populations.**O**

Acknowledgments

References

1. van Marken Lichtenbelt WD, Vanhommerig JW, Smulders NM, et al. Cold-activated brown adipose tissue in healthy men. *N Engl J Med* 2009;360:1500-1508.
2. Virtanen KA, Lidell ME, Orava J, et al. Functional brown adipose tissue in healthy adults. *N Engl J Med* 2009;360:1518-1525.
3. Cypess AM, Lehman S, Williams G, et al. Identification and importance of brown adipose tissue in adult humans. *N Engl J Med* 2009;360:1509-1517.
4. Holstila M, Pesola M, Saari T, et al. MR signal-fat-fraction analysis and T2* weighted imaging measure BAT reliably on humans without cold exposure. *Metabolism* 2017;70:23-30.
5. Symonds ME, Henderson K, Elvidge L, et al. Thermal imaging to assess age-related changes of skin temperature within the supraclavicular region co-locating with brown adipose tissue in healthy children. *J Pediatr* 2012;161:892-898.
6. Nedergaard J, Bengtsson T, Cannon B. Unexpected evidence for active brown adipose tissue in adult humans. *Am J Physiol Endocrinol Metab* 2007;293:E444-E452.
7. Leitner BP, Huang S, Brychta RJ, et al. Mapping of human brown adipose tissue in lean and obese young men. *Proc Natl Acad Sci U S A* 2017;114:8649-8654.
8. Law J, Morris DE, Izzi-Engbeaya C, et al. Thermal imaging is a noninvasive alternative to PET/CT for measurement of brown adipose tissue activity in humans. *J Nucl Med* 2018;59:516-522.
9. Chen YC, Cypess AM, Chen YC, et al. Measurement of human brown adipose tissue volume and activity using anatomic MR imaging and functional MR imaging. *J Nucl Med* 2013;54:1584-1587.
10. Franz D, Karampinos DC, Rummeny EJ, et al. Discrimination between brown and white adipose tissue using a 2-point Dixon water-fat separation method in simultaneous PET/MRI. *J Nucl Med* 2015;56:1742-1747.
11. Franz D, Weidlich D, Freitag F, et al. Association of proton density fat fraction in adipose tissue with imaging-based and anthropometric obesity markers in adults. *Int J Obes (Lond)* 2018;42:175-182.
12. McCallister D, Zhang L, Burant A, Katz L, Branca RT. Effect of microscopic susceptibility gradients on chemical-shift-based fat fraction quantification in supraclavicular fat. *J Magn Reson Imaging* 2019;49:141-151.
13. Franz D, Diefenbach MN, Treibel F, et al. Differentiating supraclavicular from gluteal adipose tissue based on simultaneous PDFF and T₂ * mapping using a 20-echo gradient-echo acquisition [published online January 25, 2019]. *J Magn Reson Imaging.* doi:10.1002/jmri.26661
14. Cypess AM, Chen YC, Sze C, et al. Cold but not sympathomimetics activates human brown adipose tissue in vivo. *Proc Natl Acad Sci U S A* 2012;109:10001-10005.
15. Kobata K, Sutoh K, Todo T, Yazawa S, Iwai K, Watanabe T. Nordihydrocapsiate, a new capsinoid from the fruits of a nonpungent pepper, capsicum annuum. *J Nat Prod* 1999;62:335-336.
16. Snitker S, Fujishima Y, Shen H, et al. Effects of novel capsinoid treatment on fatness and energy metabolism in humans: possible pharmacogenetic implications. *Am J Clin Nutr* 2009;89:45-50.
17. Yoneshiro T, Aita S, Kawai Y, Iwanaga T, Saito M. Nonpungent capsaicin analogs (capsinoids) increase energy expenditure through the activation of brown adipose tissue in humans. *Am J Clin Nutr* 2012;95:845-850.
18. Sun L, Camps SG, Goh HJ, et al. Capsinoids activate brown adipose tissue (BAT) with increased energy expenditure associated with subthreshold 18-fluorine fluorodeoxyglucose uptake in BAT-positive humans confirmed by positron emission tomography scan. *Am J Clin Nutr* 2018;107:62-70.
19. Inoue N, Matsunaga Y, Satoh H, Takahashi M. Enhanced energy expenditure and fat oxidation in humans with high BMI scores by the ingestion of novel and non-pungent capsaicin analogues (capsinoids). *Biosci Biotechnol Biochem* 2007;71:380-389.
20. Goh HJ, Govindharajulu P, Camps SG, Tan SY, Henry CJ. Gross and relative energy cost of domestic household activities in Asian men. *Eur J Clin Nutr* 2016;70:1414-1419.
21. Hu HH, Yin L, Aggabao PC, Perkins TG, Chia JM, Gilsanz V. Comparison of brown and white adipose tissues in infants and children with chemical-shift-encoded water-fat MRI. *J Magn Reson Imaging* 2013;38:885-896.
22. Zhong X, Nickel MD, Kannengiesser SA, Dale BM, Kiefer B, Bashir MR. Liver fat quantification using a multi-step adaptive fitting approach with multi-echo GRE imaging. *Magn Reson Med* 2014;72:1353-1365.
23. Gifford A, Towse TF, Walker RC, Avison MJ, Welch EB. Human brown adipose tissue depots automatically segmented by positron emission tomography/computed tomography and registered magnetic resonance images. *J Vis Exp* 2015:e52415. doi:10.3791/52415
24. Maes F, Collignon A, Vandermeulen D, Marchal G, Suetens P. Multimodality image registration by maximization of mutual information. *IEEE Trans Med Imaging* 1997;16:187-198.
25. Schindelin J, Rueden CT, Hiner MC, Eliceiri KW. The ImageJ ecosystem: an open platform for biomedical image analysis. *Mol Reprod Dev* 2015;82:518-529.
26. Yushkevich PA, Piven J, Hazlett HC, et al. User-guided 3D active contour segmentation of anatomical structures: significantly improved efficiency and reliability. *Neuroimage* 2006;31:1116-1128.
27. McCallister A, Zhang L, Burant A, Katz L, Branca RT. A pilot study on the correlation between fat fraction values and glucose uptake values in supraclavicular fat by simultaneous PET/MRI. *Magn Reson Med* 2017;78:1922-1932.
28. Schmid B, Schindelin J, Cardona A, Longair M, Heisenberg M. A high-level 3D visualization API for Java and ImageJ. *BMC Bioinformatics* 2010;11:274. doi:10.1186/1471-2105-11-274
29. Ang QY, Goh HJ, Cao Y, et al. A new method of infrared thermography for quantification of brown adipose tissue activation in healthy adults (TACTICAL): a randomized trial. *J Physiol Sci* 2017;67:395-406.
30. Lean ME. Brown adipose tissue in humans. *Proc Nutr Soc* 1989;48:243-256.
31. Astrup A, Bülow J, Christensen NJ, Madsen J. Ephedrine-induced thermogenesis in man: no role for interscapular brown adipose tissue. *Clin Sci (Lond)* 1984;66:179-186.
32. Astrup A, Bülow J, Madsen J, Christensen NJ. Contribution of BAT and skeletal muscle to thermogenesis induced by ephedrine in man. *Am J Physiol* 1985(5 Pt 1);248:E507-E515.
33. Chen KY, Cypess AM, Laughlin MR, et al. Brown Adipose Reporting Criteria in Imaging Studies (BARCIST 1.0): recommendations for standardized FDG-PET/CT experiments in humans. *Cell Metab* 2016;24:210-222.
34. Schade KN, Baranwal A, Liang C, Mirbolooki MR, Mukherjee J. Preliminary evaluation of β3-adrenoceptor agonist-induced 18F-FDG metabolic activity of brown adipose tissue in obese Zucker rat. *Nucl Med Biol* 2015;42:691-694.
35. Mirbolooki MR, Upadhyay SK, Constantinescu CC, Pan ML, Mukherjee J. Adrenergic pathway activation enhances brown adipose tissue metabolism: a [¹⁸F]FDG PET/CT study in mice. *Nucl Med Biol* 2014;41:10-16.
36. van Rooijen BD, van der Lans AA, Brans B, et al. Imaging cold-activated brown adipose tissue using dynamic T2*-weighted magnetic resonance imaging and 2-deoxy-2-[18F]fluoro-D-glucose positron emission tomography. *Invest Radiol* 2013;48:708-714.
37. Koskensalo K, Raiko J, Saari T, et al. Human brown adipose tissue temperature and fat fraction are related to its metabolic activity. *J Clin Endocrinol Metab* 2017;102:1200-1207.
38. Raiko J, Holstila M, Virtanen KA, et al. Brown adipose tissue triglyceride content is associated with decreased insulin sensitivity, independently of age and obesity. *Diabetes Obes Metab* 2015;17:516-519.